

Northeastern University
Electrical and Computer Engineering Department
ECE U792 Capstone Design 2

Magneto-Optical Kerr Effect Microscope

Faculty Advisors

Professor Charles DiMarzio, Professor Nian Sun

Design Team

Adam Brandow, Anton Geiler, Paul Head, Rui Loura, Heath Marvin, Michael Zartarian

Sponsor

Center of Microwave Magnetic Materials and Integrated Circuits

Table of Contents

| | |
|--|----|
| Magnetic Domains | 1 |
| Domain Observation Techniques..... | 1 |
| Magneto-Optical Kerr Effect Microscopy | 1 |
| Magneto-Optical Kerr Effect | 2 |
| Visual Contrast Optimization | 4 |
| Applications | 6 |
| Other Methods | 6 |
| Optical Design | 8 |
| Optics | 8 |
| Angle of Incidence | 9 |
| Zemax Simulation..... | 10 |
| Field of View and Resolution | 11 |
| Light Source..... | 12 |
| Dithering | 12 |
| Optical Construction | 16 |
| Electromagnet | 18 |
| Power Supply | 19 |
| Equipment Interfaces | 20 |
| Control Loop..... | 21 |
| Camera Interface | 21 |
| Digital Image Processing | 22 |
| User Interface..... | 22 |
| Sample Preparation | 25 |
| Results and Discussion | 26 |
| Summary | 28 |
| Acknowledgements..... | 28 |

List of Figures

| | |
|---|----|
| Figure 1 – Domain pattern (left) and the substructure of the domain walls (right) on a (100)-oriented SiFe crystal. | 1 |
| Figure 2 - Vector diagram for the longitudinal magneto-optical Kerr effect. K vector is the Kerr amplitude generated as a result of interaction of the light beam with the magnetization vector M. | 2 |
| Figure 3 - Irradiance dependence on analyzer setting θ in degrees | 5 |
| Figure 4 - Mitutoyo FS110 Inspection Microscope [6] | 8 |
| Figure 5: MOKE Microscope light path | 9 |
| Figure 6: ZeMax simulation using actual microscope lenses. | 10 |
| Figure 7: Spot size and collimated beam with paraxial lens..... | 11 |
| Figure 8: Magnetic Recording Head Prior to Dithering | 13 |
| Figure 9: Light Mode Propagation in Multimodal Fiber | 13 |
| Figure 10: Mechanical Dithering | 14 |
| Figure 11: Optical Dithering, Rotating Plastic Sheets at Output Coupling | 15 |
| Figure 12: Magnetic Recording Head After Dithering | 15 |
| Figure 13: Infinity Space Expansion..... | 16 |
| Figure 14: Micrometer Stages mounted to the side of the breadboard | 17 |
| Figure 15: Sample Biasing Electromagnet | 18 |
| Figure 16: Kepco BOP 20-10M Bi-polar Power Supply | 20 |
| Figure 17: Lakeshore 421 Gaussmeter | 20 |
| Figure 18: Software User Interface..... | 23 |
| Figure 19: Photolithographic mask..... | 25 |
| Figure 20: (a) Raw image, (b) Background subtracted image, (c) Digitally processed image..... | 26 |
| Figure 21: Magnetic domain images shown in RGB colormap..... | 27 |

Magnetic Domains

In order to gain insight into the properties of magnetic materials and devices it is important to be able to study the magnetic domain structure of the material or device under investigation. Magnetic domains are regions of unidirectional magnetization which are governed by one of the fundamental laws of nature – minimization of energy in the system. Invisible to the naked eye, these are microscopic structures within otherwise unstructured magnetic materials (Figure 1). The understanding of the structure and dynamics of magnetic domains is becoming increasingly important in various applications of magnetic materials, such as thin-film recording heads in the magnetic recording industry and spin-electronic devices in information technology.

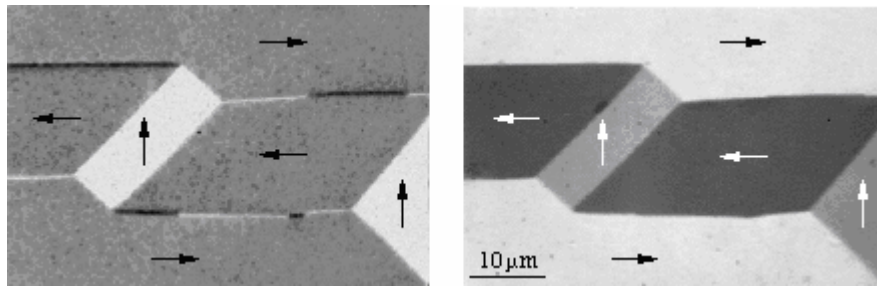


Figure 1 – Domain pattern (left) and the substructure of the domain walls (right) on a (100)-oriented SiFe crystal.

Domain Observation Techniques

A number of different techniques to study the domain structure of magnetic materials exist today. One of these techniques is the magneto-optical imaging technique which has significant advantages of being relatively inexpensive, non-invasive, non-contaminating, and able to handle a broad range of magnetic samples. Magneto-optical imaging in reflective mode takes advantage of the magneto-optical Kerr Effect while imaging in transmission mode takes advantage of the Faraday Effect. The underlying principle of both effects is similar. The light reflected from the surface of a magnetic sample or transmitted through a magnetic sample will interact with the magnetization within the sample. Through this interaction, the polarization state of the light will change and the difference between the incident and reflected (transmitted) beams can be used to study the magnetization within different regions of the sample.

Magneto-Optical Kerr Effect Microscopy

In our Capstone project we built a Magneto-Optical Kerr Effect Microscope which will be used in development and characterization of magnetic materials and devices in the Center of Microwave Magnetic Materials and Integrated Circuits at Northeastern University. The project will initially concentrate on the study of thin metallic magnetic films which exhibit a more pronounced magneto-optical effect producing a stronger signal which is easier to detect and analyze. Depending on the progress in this stage of the project we also intend to extend our inquiry into materials which present more challenges in Kerr Effect Microscopy such as ceramic thin films and bulk samples.

Optimum optical contrast conditions for different materials are obtained through three major types of magneto-optical Kerr effect. These types are classified into polar, longitudinal, and transverse Kerr effects depending on the vector relationships between incident light polarization, plane of incidence, and the magnetization within the sample. An example of directional relationships between these physical quantities is shown in Figure 2 for the longitudinal case.

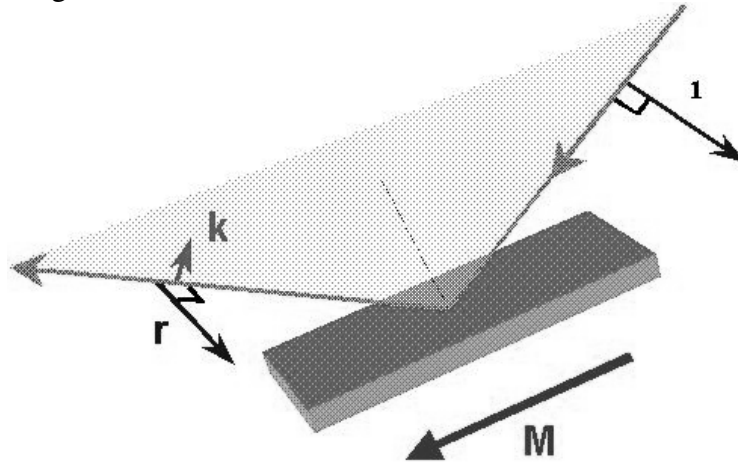


Figure 2 - Vector diagram for the longitudinal magneto-optical Kerr effect. K vector is the Kerr amplitude generated as a result of interaction of the light beam with the magnetization vector M.

Magneto-Optical Kerr Effect

In order to detect the changes introduced into the polarization state of the light by reflection from a magnetized surface a pair of nearly crossed polarizers is located in the optical path. The linear polarizer on the incident beam restricts the polarization to one direction. Through the interaction of the light with the magnetized surface polarization components perpendicular to that of the incident beam are generated. The reflected beam is passed through an analyzer which is nearly crossed with the incident light polarizer. As a result, the component of the light that maintained its original polarization state after the interaction with the magnetized surface is attenuated while the component generated through the magneto-optical (Kerr) interaction is allowed to pass to the detector [1].

Maximum attenuation of the incident light is achieved when the polarizers are perfectly crossed, however Kerr component of the light is very weak and would require an extremely sensitive detector. By allowing some of the incident light to reach the detector the Kerr signal and the background (incident) signal are allowed to add coherently contributing to a higher signal which is easily registered by conventional detectors [2]. The magneto-optical Kerr effect is conveniently described by Jones matrix approach. The incident light beam is described by the following polarization vector:

$$\vec{E} = \begin{bmatrix} E_x \\ E_y \end{bmatrix} \quad (1)$$

We can represent the polarizer on the incident beam by the following matrix (assuming ideal polarizer for simplicity):

$$\bar{P} = \begin{bmatrix} 0 & 1 \\ 0 & 0 \end{bmatrix} \quad (2)$$

In this setup, the light incident upon the magnetized surface will have linear polarization in the y-direction. The analyzer set to angle Θ from the x-direction (for $\Theta = 0$ the two polarizers will be perfectly crossed):

$$\bar{A} = \begin{bmatrix} \cos^2 \Theta & -\cos \Theta \sin \Theta \\ -\cos \Theta \sin \Theta & \sin^2 \Theta \end{bmatrix} \quad (3)$$

The interaction of the light with the magnetized surface can be represented as a summation of the oblique reflection matrix and the magneto-optical effect matrix [3]:

$$\bar{J} = \begin{bmatrix} \rho_{SS} & 0 \\ 0 & \rho_{PP} \end{bmatrix} + \begin{bmatrix} 0 & \rho_{SP}^L(Q_V) \sin \phi \\ -\rho_{SP}^L(Q_V) \sin \phi & \rho_{PP} \sin^2 \phi + \rho_{PP}^T(Q_V / \cos \phi) \cos^2 \phi \end{bmatrix} \quad (4)$$

In the above expression the first term represents the oblique reflection matrix where ρ_{SS} and ρ_{PP} are the Fresnel coefficients for correspondingly polarized light components. The second term describes the magneto-optical effect where ρ_{SP}^L and ρ_{PP}^T are the reflection coefficients responsible for the Kerr rotation of the polarization state of the light, ϕ is the angle between the magnetization vector and the plane of incidence, and Q_V is the complex Voigt magneto-optical constant. For the longitudinal Kerr effect equation (4) simplifies to:

$$\bar{J} = \bar{J}_0 + \bar{J}_1 = \begin{bmatrix} \rho_{SS} & 0 \\ 0 & \rho_{PP} \end{bmatrix} + \begin{bmatrix} 0 & \rho_{SP}^L(Q_V) \\ -\rho_{SP}^L(Q_V) & 0 \end{bmatrix} \quad (5)$$

The magneto-optical reflection coefficient ρ_{SP}^L for the longitudinal case is given by [4]:

$$\rho_{SP}^L = \frac{-in \cos \theta_0 m_y \sin \theta_1 Q_V}{(n \cos \theta_0 + \cos \theta_1)(\cos \theta_0 + n \cos \theta_1) \cos \theta_1} \quad (6)$$

In this case, the light is incident from air at an angle θ_0 upon a magnetic medium with index of refraction n . The magnetization is given by m_y in the y-direction. The angle of refraction within the magnetic medium θ_1 is obtained by application of Snell's Law. Combining the above components we can summarize the input-output relationship of the magneto-optical Kerr effect microscope as follows:

$$\vec{E}_{OUT} = \bar{A} \cdot (\bar{J}_0 + \bar{J}_1) \cdot \vec{E}_{IN} \quad (7)$$

Based on equation 6 we can now write the power relationship for normalized electric field amplitudes:

$$\|\vec{E}_{OUT}\|^2 = \vec{E}_{OUT}^T \vec{E}_{OUT} = \vec{E}_{IN}^T \cdot (\bar{J}_0^T + \bar{J}_1^T) \cdot \bar{A}^T \cdot \bar{A} \cdot (\bar{J}_0 + \bar{J}_1) \cdot \vec{E}_{IN} \quad (8)$$

Equation 7 contains 4 terms as follows:

$$\begin{aligned}
\|\vec{E}_{OUT}\|^2 = & \vec{E}_{IN}^T \cdot \vec{J}_0^T \cdot \vec{A}^T \cdot \vec{A} \cdot \vec{J}_0 \cdot \vec{E}_{IN} + \\
& \vec{E}_{IN}^T \cdot \vec{J}_0^T \cdot \vec{A}^T \cdot \vec{A} \cdot \vec{J}_1 \cdot \vec{E}_{IN} + \\
& \vec{E}_{IN}^T \cdot \vec{J}_1^T \cdot \vec{A}^T \cdot \vec{A} \cdot \vec{J}_0 \cdot \vec{E}_{IN} + \\
& \vec{E}_{IN}^T \cdot \vec{J}_1^T \cdot \vec{A}^T \cdot \vec{A} \cdot \vec{J}_1 \cdot \vec{E}_{IN}
\end{aligned} \tag{9}$$

The first three terms in equation 9 will determine the intensity ratio between the background component of the light and the Kerr effect component of the light. Hence these terms are critical in optimizing the contrast when an image of the magnetic domain structures is captured with a digital camera. First term will determine the background light intensity while the two subsequent terms will determine the intensity of the Kerr effect light.

Visual Contrast Optimization

To gain quantitative insight into the advantages of slightly uncrossing the incident and the reflected light polarizers in the light path of the Kerr effect microscope consider the following simplified form of equation 9:

$$\left| \vec{E}_0 + \vec{E}_K \right|^2 = \left| \vec{E}_0 \right|^2 + \vec{E}_0 \vec{E}_K^* + \vec{E}_0^* \vec{E}_K + \left| \vec{E}_K \right|^2 \tag{10}$$

Here, \vec{E}_0 is the amplitude of the reflected light which maintained the original polarization state after the incidence (background) and \vec{E}_K is the amplitude of the Kerr component of the reflected light. These terms were organized in the order corresponding to the terms of equation 9. Hence, the first term represents the irradiance of the background signal, the second and the third terms (conjugate pair) represent the coherent addition of the Kerr signal and the background signal while the third term is the irradiance of the Kerr component of the light. To make this analysis more quantitative we considered a high permeability metallic Permalloy film (Ni-Fe alloy). This film represents a major challenge in magneto-optical investigations due to very weak polarization rotations. The Kerr rotation angle defined by the arcsine of the ratio between Kerr and background components of the light was reported to be on the order of 0.001° for Permalloy films [5]. Consequently, the irradiance of the Kerr component of the light is on the order of 10^{-6} with respect to the irradiance of the background component of the light. With such a ratio, generating a visual contrast was quite challenging. However, due to the coherent nature of the addition of the Kerr and the background components of the light much higher contrast can be generated due to the second and the third terms in equations 9 and 10. This approach is represented graphically in Figure 3:

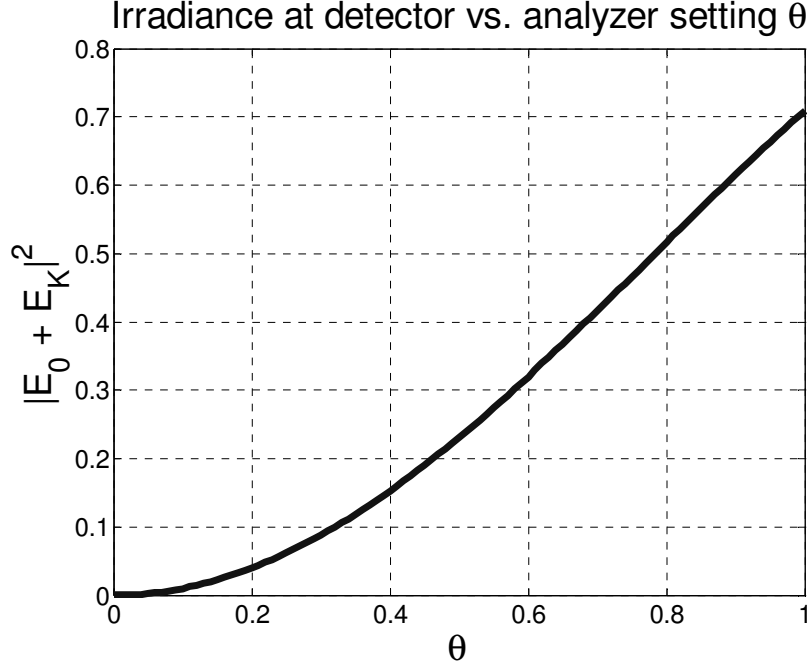


Figure 3 - Irradiance dependence on analyzer setting θ in degrees

The background light amplitude \vec{E}_0 is proportional to $\sin(\theta)$ where θ is the analyzer setting (as expected for $\theta = 0$ perfect extinction of the background light occurs). Consequently, for fixed Kerr amplitude \vec{E}_K the irradiance detected after the analyzer exhibits a parabolic dependence on the angle θ . Since the slope of the curve in Figure 3 increases with increasing θ , for higher values of θ a small change in the Kerr amplitude \vec{E}_K will produce a higher change in the detected irradiance. Based on this observation we can conclude that by increasing the angle θ we can increase the visual contrast introduced into the image by the appearance of the Kerr signal. This conclusion can also be verified by substituting the dependence of the background light intensity and the relative Kerr amplitude into equation 10. The ratio between the background irradiance and the Kerr component irradiance is then given by:

$$DR = \frac{|\vec{E}_0|^2}{\vec{E}_0 \vec{E}_K^* + \vec{E}_0^* \vec{E}_K} \approx \frac{\sin^2 \theta}{\sin \theta \cdot 10^{-3}} = \frac{\sin \theta}{10^{-3}} \quad (11)$$

In this equation DR is the dynamic range of the image obtained by the magneto-optical setup described above. This is a noticeable improvement from the 10^6 ratio in the perfectly crossed polarizers scenario. In order to achieve visual contrast in magneto-optical effect imaging the Kerr signal has to be sufficient to produce several counts in the corresponding pixels of a CCD camera. In the previous example, for Permalloy film, setting the angle θ to 6° will create a dynamic range of about 100. Hence, if the experimental setup is configured such that the background light generates 200 counts in the pixels of the CCD camera the Kerr signal will contribute to $200/DR = \pm 2$ pixels (depending on the orientation of the magnetization in the given area of the sample) which will translate into visual contrast in the magneto-optical effect image. According to this analysis an 8-bit CCD camera with a count range of 0-255 will be able to produce an

image where the magnetic domain structure of the material is visible. Considering the fact that the noise level of a typical (un-intensified) CCD camera is on the order of 2-4 counts digital image processing will be required to eliminate the noise contribution to the image. Upgrading to a 10-bit CCD camera will provide a dynamic range of 1024. Configuring the experiment such that the background contributes to 900 counts will cause the Kerr effect signal to produce as many as ± 9 counts which is considerably higher than the CCD noise level. The images can be further improved by the digital image processing methods.

Based on the theoretical analysis of the magneto-optical Kerr effect microscope carried out in this section we conclude that this approach can be applied in the study and characterization of magnetic materials by providing a visual image of the magnetic domain structure of the material under investigation. Applying various biasing fields to the magnetic materials in this setup will allow us to study the dynamic behavior of magnetic domains. Case study of Permalloy has shown that visual contrast can be obtained even for this material which has proven to be particularly challenging in magneto-optical investigations due to very weak Kerr rotations.

Applications

Magnetic domain studies are instrumental in many electrical applications, including magnetic storage devices, transformers and motors. Understanding magnetic domains means higher performance and efficiency in such devices. In order to better understand these magnetic domains the Kerr effect can be used to study their structure. As the technology to manufacture the devices dependant on magnetic domains advances, so does the difficulty in observing their structure.

One such application is magnetic recording media. Now that manufacturing technologies have advanced to the point where a much thinner storage medium can be made we are able to increase the storage density of devices that use this technology. Also by decreasing the thickness of such a medium we are now able to decrease the coactivity and thus the same amount of data can be stored with a weaker magnetic field [1]. The Kerr effect microscope can be used to observe the domain walls and find the correct medium thickness and coactivity combination for a stable information element.

Other Methods

It is important to consider other the methods of observing magnetic domains besides the Kerr effect microscope. One such method is the Bitter technique which maps the stray fields of a domain pattern with the use of colloidal magnetite particles. One main disadvantage to this method is the fact that the application of the colloid to the magnetic sample could actually affect the domains and give a false image of their structure. Also it is important to note that the bitter effect measures the stray fields of magnetic domains. So when it is necessary to observe the domain structure of a higher permeable material, or any material where the stray fields are weak, the Bitter method would be less than ideal [1].

One of the main advantages of observing domains through the magneto-optical Kerr effect is that it can observe a variety of sample shapes, sizes, and compositions all while leaving it uninfluenced during observation. Another method for domain observation, Transmission Electron Microscopy [TEM], is limited in its ability to observe different shapes and sizes of samples. It is also difficult to apply outside influences, such as magnetic fields and physical stresses, to the sample while observing it [1]. The TEM also has a smaller field of view than the Kerr Microscope, which is less expensive than the TEM, and uses materials and items that can be adapted for other purposes.

The Kerr microscope is the one of the most versatile domain observations techniques considering the cost. It can observe a wide range of magnetic samples that can be used for a variety of magnetic devices. While there is other observation techniques available, one that employs the Kerr effect is an effective solution in today's modern magnetic material laboratories.

Optical Design

In the design of the optical system of the Magneto-Optical Kerr Effect Microscope we rely on some of the components integrated into the Mitutoyo FS110 Inspection Microscope (Figure 4). The microscope had several limitations which required significant modification in order to adapt it in the MOKE Microscope design. One of the main limitations was the limited infinity space available to us in the microscope.



Figure 4 - Mitutoyo FS110 Inspection Microscope [6]

While the microscope had infinity corrected optics it was not designed to allow the users to incorporate additional optical components into the frame of the microscope. In order to achieve a high signal to noise ratio and eliminate as much background light as possible we used high quality optical components. For example, a pair of polarizers (Glan-Thompson prisms) with an extinction ratio of 10^{-6} occupy a volume of 1/8 cubic inches each. Sheet polarizers previously used in the microscope have an extinction ratio of 10^{-4} at best. Additionally, the original optical path in the microscope utilized a non-polarizing beam splitter with a transmission ratio of about 50%. Such losses could not be tolerated in such a sensitive design where much of the designs success depended on the optimum light conditions. This beam splitter was replaced with a polarizing beam splitter with transmission ratio of as much as 95% which occupies a volume similar to that of Glan-Thompson prisms (~1/8 cubic inches). As a result it was decided to rebuild the component of the microscope that houses the infinity space to create more room for the necessary optical components. This brought the illumination straight into infinity space and avoided any effects introduced by transmission through various components previously installed in the microscope. In our final design, we only use a small part of the original Mitutoyo FS110. The only part that was completely unmodified was the objective lenses. We are using the translation stage—though significantly modified—and also the tube lens and camera mount. The tube lens assembly may undergo further modifications when a Bertrand lens is installed. The Bertrand lens will enable the user to locate the illumination spot in the back focal plane, and when implemented, will increase the ease of use of the microscope.

Optics

Our light source—discussed shortly—follows the path shown in Figure 5. The laser is coupled with a multimode, 0.2 NA optical fiber. After passing through the fiber, the light

passed through a collimating lens, the Glan-Thomson polarizer and a focusing lens before it is reflected down to the sample by the polarizing beam splitter. The beam is focused in the back focal plane of the objective lens and is then collimated by the objective to illuminate the sample. This illumination is provided by coherent laser light and requires dithering for uniform illumination. Dithering will be discussed in more detail later.

The light that illuminates the sample is reflected with changes in polarization, amplitude, and phase due to the magneto-optical Kerr effect. These changes are dependent on the orientation of the magnetization. This light, with its changes due to the orientation of the magnetization, is reflected back through the object, through the polarizing beam splitter and the analyzer before being focused on the CCD by the tube lens.

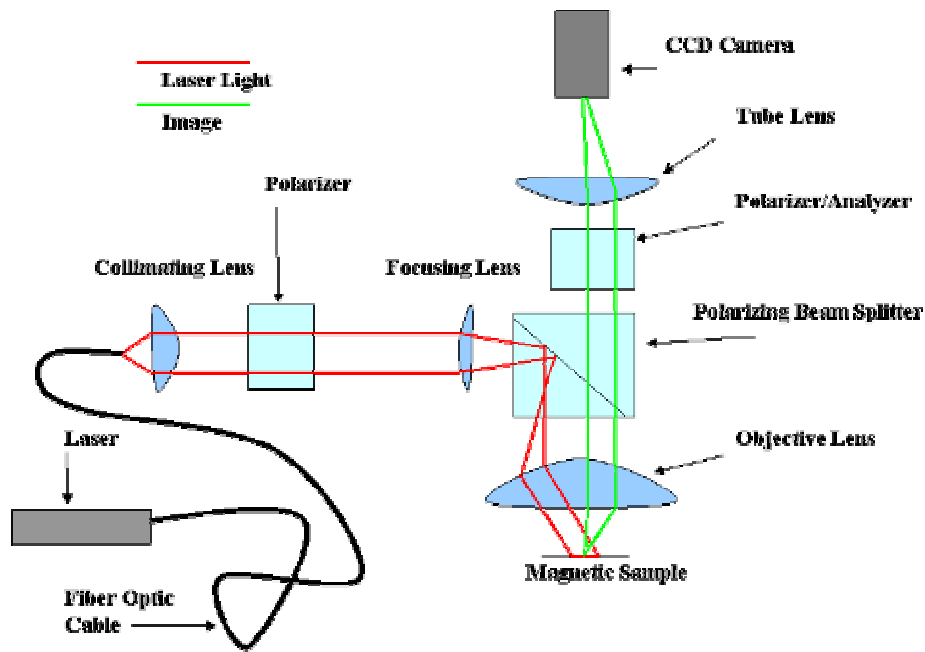


Figure 5: MOKE Microscope light path

The second polarizer, which is nearly perpendicularly crossed with the first, in combination with the polarizing beam splitter, function as a filter for the light which reflects off the sample without changes in polarization. As discussed in the previous sections on magnetism, the rotation angle of the polarization is very low (0.01 degrees or lower depending on the sample under observation), and the signal of the Kerr-affected light is therefore very weak. This weak signal passes through the second polarizer—also called the analyzer—and through the tube lens into the camera and to the image processing in the computer interface for enhancement.

Angle of Incidence

The angle of incidence of the polarized light was an element of our study. The light path diagram above shows that vertical adjustments to the tip of the fiber facilitate changes in

the angle of incidence. As mentioned in the Magneto-Optical Kerr Effect section longitudinal and transverse Kerr Effects vanish for normal incidence. Consequently, a large and well defined angle of incidence is critical in Kerr microscopy. Though it was difficult to quantitatively measure the actual angle of incidence of our design, the definition of this angle depended on the quality of our optical components and design. Theoretical limit of the angle of incidence achievable in our system is given by the numerical aperture of the given objective. In order to understand the behavior of our system, we simulated our design in Zemax, a ray tracing and analysis software.

Zemax Simulation

One of the main challenges of our optical design was producing a well collimated illumination beam out of the objective lens. The better the collimation of this beam, the more defined the angle of incidence can be. The entire optical system was simulated in Zemax using the actual lenses used in the MOKE Microscope. As is evident in Figure 6, the aberrations introduced into the light path by the short focal length of the fiber collimating lens increase the spot size in the back focal plane of the objective lens. This then reduces the collimation of the illumination beam and thus reduces the definition of the angle of incidence. It is important to note that even with this imperfection in the design, Kerr images were clearly seen.

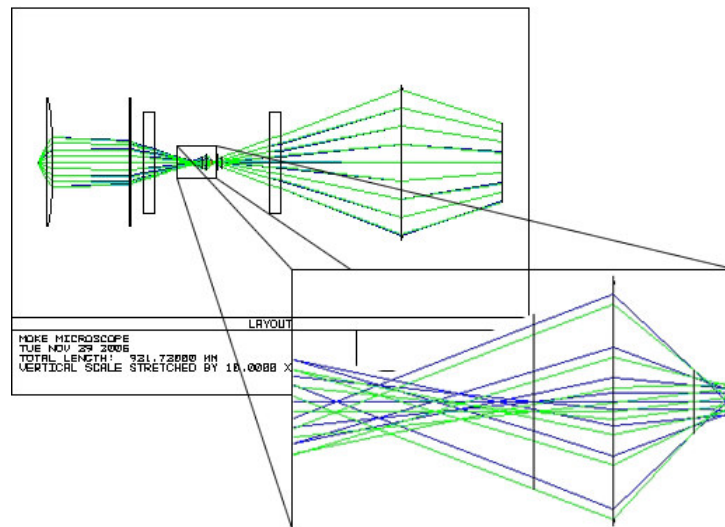


Figure 6: ZeMax simulation using actual microscope lenses.

In further simulations we replaced the collimating lens with a paraxial lens in Zemax. This provides a good approximation for a multi-element, infinity corrected lens. The resulting reduction in the spot size in the back focal plane can be seen Figure 7. Through our simulations we have shown that replacing the collimating lens after the fiber will greatly increase our angle of incidence definition and may help produce even higher contrast images.

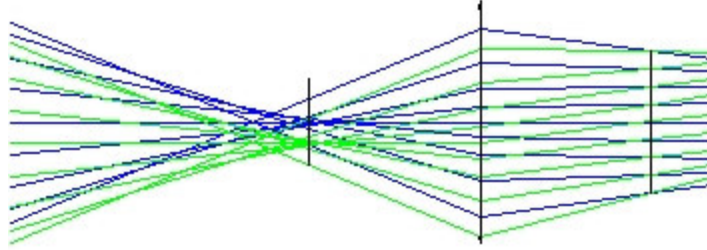


Figure 7: Spot size and collimated beam with paraxial lens.

Changing the angle of incidence allows the user to find the angle that has the largest effect on the polarization angle and thereby gives the best contrast in domain imaging. This angle flexibility is only possible if the beam size is sufficiently small and well defined. The problems that may arise with a small beam size are discussed in the following section.

Field of View and Resolution

Some of the critical parameters that were considered in the design of the optical system are the field of view and the resolution. Field of view defines the area of the sample that can be viewed simultaneously by the microscope. Desired field of view is ultimately determined by the area of the CCD chip within the digital camera. For the Scion Scientific CFW-1312M camera in our design the area of the CCD is 7.6x6.2mm. For 100x objective the field of view in object plane is determined by dividing the dimensions of the CCD by the magnification. Consequently, minimum required field of view to utilize the entire area of the CCD is 76x62 μ m.

It is undesired, however, to limit the illumination spot in the object plane to the field of view of the camera. In this case the variation in intensity of the illumination across the field of view will be significant and the resulting images will be distorted. Variations in intensity result from non-uniform distribution of energy in the light beam, where more energy is contained in the center of the beam dropping off radially. We chose to design our illumination system such that the illumination spot in the object plane is bigger than the field of view of the camera by a factor of 2. This produced relatively uniformly illuminated images.

In order to achieve the illumination spot requirements the fiber output coupling optics had to be designed to allow for a collimated beam diameter that would fill the entire clear aperture of the Glan-Thompson polarizers. Since the optical fiber has a high numerical aperture (0.20) a short focal length lens had to be introduced to collimate the exiting beam. As mentioned previously, the collimated beam has to be focused to a very small point in the back focal plane of the objective lens. The alignment of the illumination focusing lens has proven to be critical to prevent intensity variations in the object plane for different incidence angle conditions.

Resolution is a critical parameter of our microscope since the domain structures for certain materials of interest can be on the order of microns or even fractions of a micron. Due to the diffraction limit, the resolution is ultimately limited by the numerical aperture of the objective lens. Consequently, for x100 objective lens (NA = 0.7) the maximum achievable resolution is given by the following equation:

$$\Delta X = \frac{C * \lambda}{NA} \quad (2)$$

to be 0.55 μ m (C assumed to be 0.61, wavelength of 633nm and 0.7 NA). In order to verify our theoretical expectations the resolution was measured experimentally once the design of the optical path was complete. To this end, several diffraction gratings were used. The gratings contained triangular edges spaced 0.5 μ m and 0.8 μ m apart. Our microscope was able to resolve the 0.8 μ m grating very clearly but could not resolve the 0.5 μ m grating. This is in good agreement with our theoretical expectations because for the x100 objective which was used in this investigation the ultimate diffraction limit related to the numerical aperture of the objective is 0.55 μ m as mentioned previously. Hence 0.8 μ m is well within microscope's resolving power; however 0.5 μ m is just outside the range.

Light Source

Because the extinction ratio required for MOKE microscopy is so high, a very intense light source is required. Traditionally, various arc sources, such as Mercury or Xenon are utilized. These sources have a disadvantage of having a multi-line or continuous spectrum, which means that bandpass filters need to be used to select appropriate wavelengths, which cuts down the available power. To address these issues we decided to utilize a laser light source in our microscope. We chose red HeNe laser, which is polarized but not stabilized (varies in intensity up to 5%). Since high quality linearly polarized light is required for MOKE microscopy the output of the laser is passed through a highly efficient polarizer. Hence, any fluctuations in the polarization state of the laser will translate into intensity variations at the output of the polarizer. We selected a polarized HeNe laser to prevent such variations which occur due to thermal changes or long term drift in the laser.

Dithering

In order to properly illuminate the samples we plan to inspect with the Magneto Optical Kerr Effect Microscope we needed to use a laser light source. The use of this source introduced a few imaging issues. Of our main concern was the presence of speckle in our image. Speckle is the presence of strong white or black regions in the image (See Figure 8). It is caused by the inherent coherence of a laser light source. A laser emits light rays or modes whose wavelengths are either completely in phase or completely out of phase. This causes many of the modes to be either fully constructive or fully destructive, hence the black or white regions (speckle). The only way to clear up this distortion of the

image is to affect the light's propagation medium in a way that would scramble the phases of the modes. There are a few different ways to do this, and we experimented with a few of them.

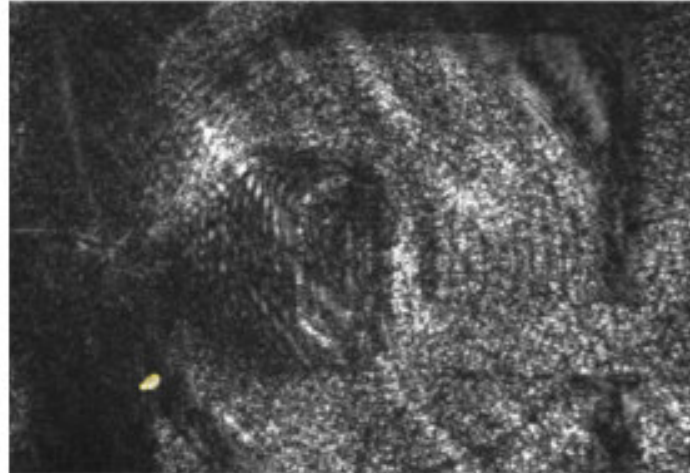


Figure 8: Magnetic Recording Head Prior to Dithering

First we decided to use multimodal fiber as the propagation medium. When light hits the input coupling of the multimodal fiber each mode enters with a slightly different reflection angle (See Figure 9).



Figure 9: Light Mode Propagation in Multimodal Fiber

This variation in reflection changes each individual mode's propagation delay slightly, so when the light exits the fiber the modes are somewhat out of phase.

The use of a multimodal fiber allowed us to use some other dithering techniques. One was intended to simulate a technique called microbending. To accomplish this we attached a few coils of the fiber to the cones of a speakers suspended from springs (See Figure 10). We then operated the speakers at a constant tone, so as to vibrate the fiber. This vibration caused a randomization in the reflection angles of the modes as they traveled down the fiber. This randomization caused the phases of the modes to be more evenly distributed when the light exited the fiber and entered the microscope.

The challenge here was finding a frequency to operate the speakers at that would cause the most even distribution possible. While viewing the image through the CCD camera, we tested a wide range of frequencies. Starting at only a few Hertz, we found that as we

increased the frequency the speckle started to disappear. Once we increased beyond 200Hz the speckle started to return. From there we tested almost all frequencies in multiples of 50 (and a few random ones) up to about 10 kHz. We found that any frequency over 250Hz did almost nothing for speckle reduction. Thus we deduced that a frequency of 200Hz would cause the most even distribution of modes.



Figure 10: Mechanical Dithering

Although the image obtained using the vibration dithering technique was a vast improvement upon our original image, it still was not acceptable for our purpose. We started to explore the possibility of randomizing the refraction angles at the input and output coupling of the fiber. After a fair amount of research we came upon a few solutions. One included mounting a wedge of glass perpendicular to the light path at either end of the fiber, and rotating it to introduce the randomization we desired. We also explored the possibility of passing the light through constantly moving nearly transparent plastic sheet of varying thickness. However there were design issues with each idea. The more we explored the rotating wedge idea the more we realized that it would be too expensive in both time, and money, and there did not seem to be a suitable way of performing a proof of concept test prior to taking on the endeavor.

Thus we started to explore the plastic sheet idea. We found some plastic sheets and started to physically shake them at the output coupling of the laser. The result was a clear improvement in the image quality. Since we needed a more automated way of achieving randomization with the plastic sheet idea, we decided to rotate the sheet at a high speed using a small electric motor (See Figure 11). In effect we combined the two ideas of rotating glass wedge and plastic sheet.

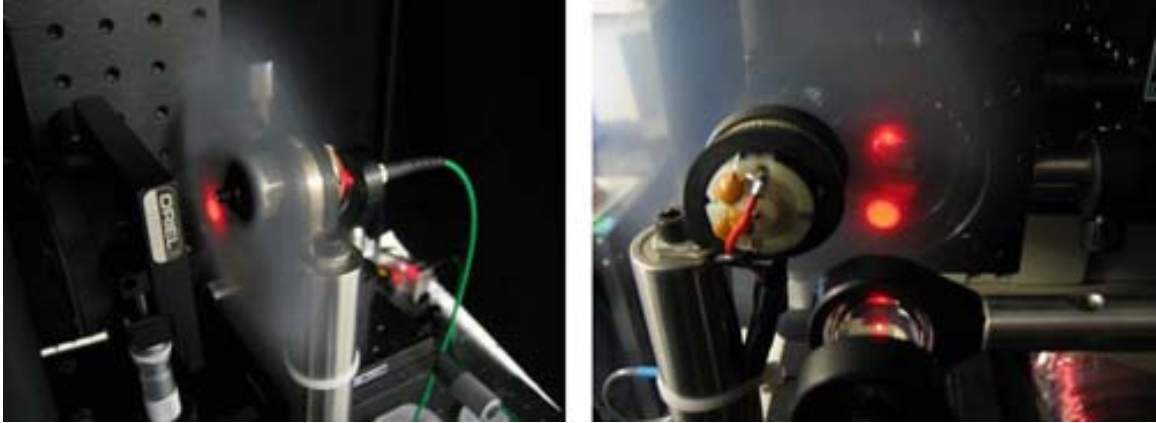


Figure 11: Optical Dithering, Rotating Plastic Sheets at Output Coupling

We introduced the design seen above at the input coupling of the fiber as well. All of these dithering techniques combined were able to provide us the image quality that we required (See Figure 12).

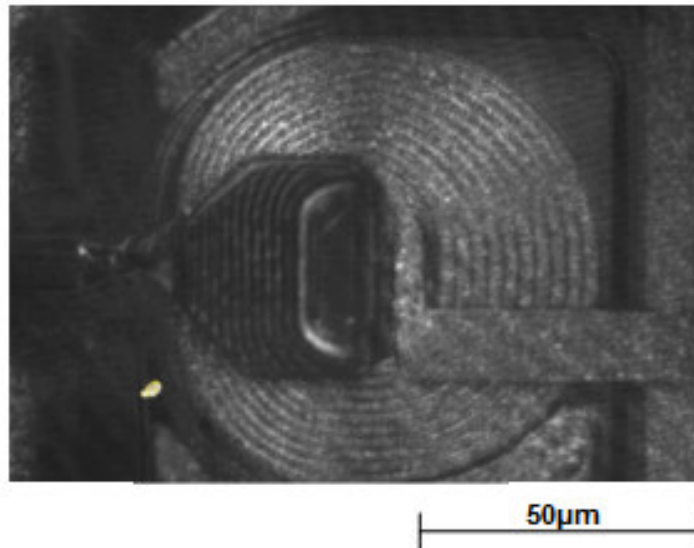


Figure 12: Magnetic Recording Head After Dithering

Optical Construction

The high precision optics called for a very stable structure to house them. In designing a structure to hold the optical components, special care had to be taken to ensure that the assembly:

- Would not drift over time
- Could be easily precisely adjusted
- Would not interfere with the electromagnet or light path
- Could be easily assembled and disassembled

The first task was to fabricate aluminum adapter to mount the original microscope to the optical table. These supports adapted into non-essential screw mounts on the original Mitutoyo.

The expansion of the infinity space was achieved by copying the internal fittings of the original microscope and then fabricating two aluminum plates that created a sufficient amount of room. Support was provided in the front by metal posts, in back the optical breadboard acted as a structural support. This made the housing very strong, and minimized the number of parts and screws needed to assemble and disassemble it. Inside this area, the polarizer, analyzer, collimator and beam splitter are mounted.

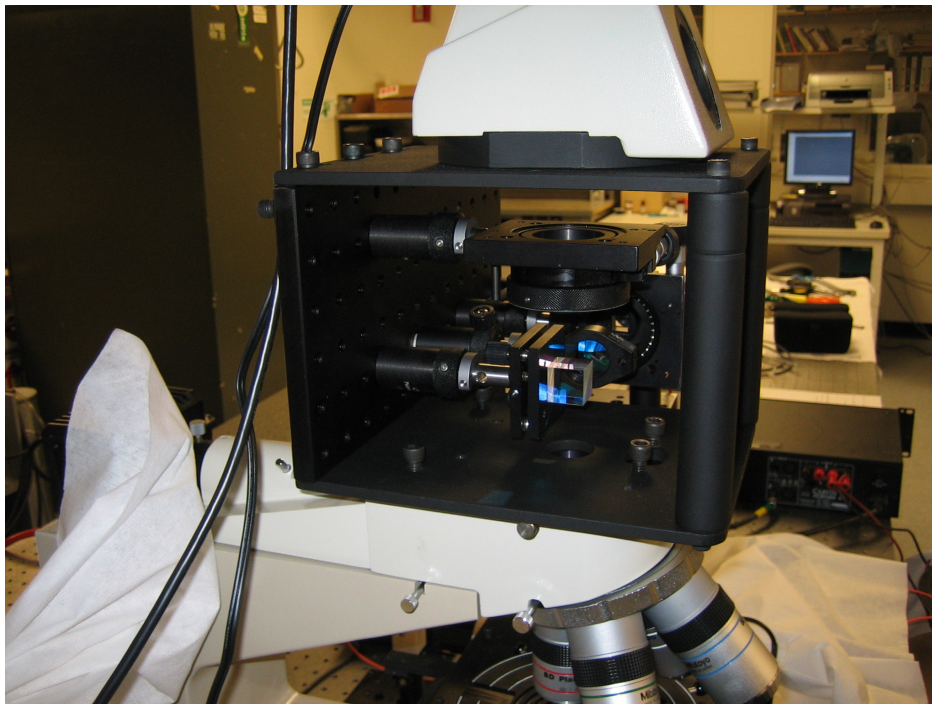


Figure 13: Infinity Space Expansion

Extending from the breadboard are several micrometer optical stages used to set the precise location of the beam. These devices are used to determine and set the Kerr

angle. Special care had to be taken to make sure the weight of these components would not compromise the rest of the structure.

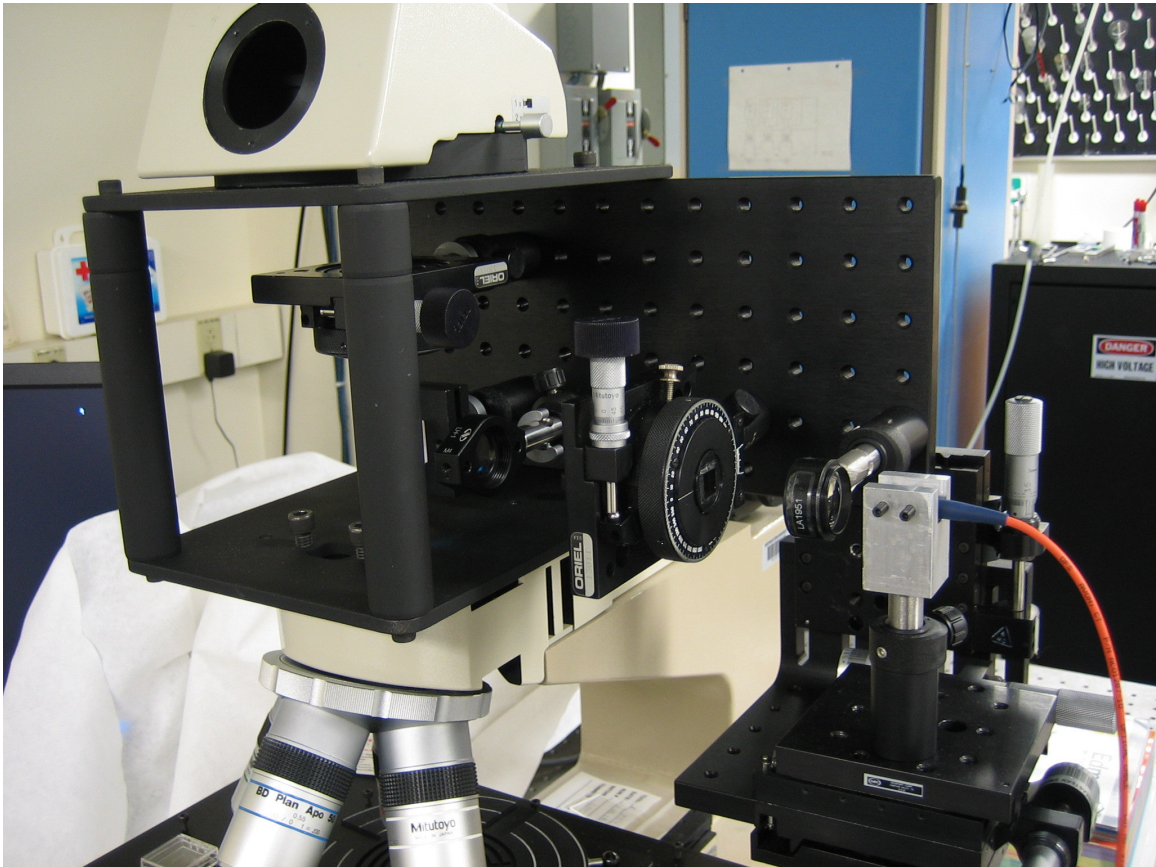


Figure 14: Micrometer Stages mounted to the side of the breadboard

Electromagnet

To correctly bias the magnetic samples, a C-shaped electromagnet was constructed.

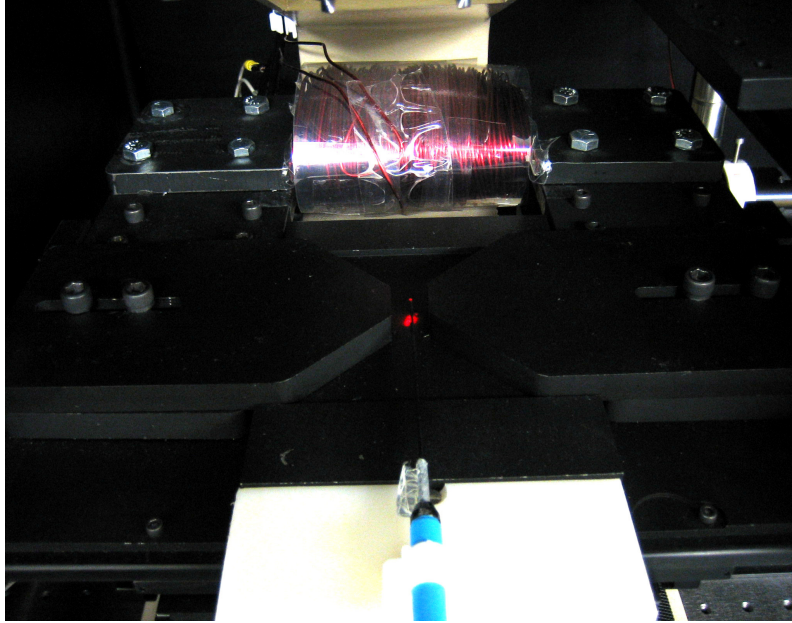


Figure 15: Sample Biasing Electromagnet

The magnet's requirements were as follows:

- Ability to apply a max field of over 2kG to work with both metallic and ceramic films
- Be able to run continuously without overheating for at least one hour at full field
- Have movable pole pieces to easily adjust maximum field and gap width
- Have flat pole pieces to place sample wafers in fringing field
- Be able to mount easily into the existing microscope sample stage

Approximate magnetic field strength calculations were made using the basic relation of ampere's law:

$$B * \text{gap length} = \mu * N * I$$

B is in Tesla (10,000 gauss)

gap is in meters (This is the opening of the "C".)

$$\mu = 4\pi * 10^{-7}$$

N is an integer equal to the number of turns in coil

I is the current in Amps

To attain a 2kG field with a small gap of 5mm, approximately 1000 ampere-turns were required. Vacuum purified soft iron was chosen as a core material for its very high saturation point. Several pieces of iron were machined and bolted together to form the core section. Some material was removed to accommodate the coil on the back section. During the construction, the coil was physically insulated from the core using special glass insulation tape.

Table 1: DC Magnetic Properties of Purified Iron

| | |
|----------------------|-------------|
| Saturation Induction | 21.5kGauss |
| Maximum Permeability | 10,000 |
| Coercive Force | 1.0 Oersted |

To reduce the labor of winding, it was chosen to wind approximately 600 turns of 14 AWG magnet wire onto the core. Thicker low-gauge wire also ensured optimal temperature performance. The finished magnet has the following specifications:

Table 2: Finished Magnet Specifications and Characteristics

| | |
|------------------------------------|-------------------------------------|
| Maximum Attainable Field (5mm gap) | 2500 Gauss |
| Max Coil Current | 10 A |
| Nominal Coil DC Resistance | ~2 Ω |
| Magnetic Core Type | Vacuum Purified Iron |
| Coil Wire Type | 14AWG Nomex Insulated 155C Class |
| Number of Wire Turns | 600 |
| Max Continuous Operating Time | 90 Minutes @ 10A (Core Temp of 50C) |
| Pole Piece Dimensions | 2cm wide x 1cm high |
| Core Dimensions | Approx. 10cm x 1cm |
| Remnant Magnetization | Approx 40 Gauss |
| Total Assembled Weight | Approx 35 lbs. |

The magnet was mounted to the microscope sample stage using a custom machined aluminum plate. This housing mated with the existing stage for a precise fit. Care was taken to ensure several centimeters of obstruction-free travel for the stage in all directions. Additionally, the large metal piece served as an excellent heat sink. To prevent corrosion, the entire assembly was painted flat black.

Power Supply

To interface with the electromagnet, a 20 volt, 10 ampere bi-polar supply was needed. This supply also needed to have easy integration into LabVIEW. We selected the Kepco BOP 20-10M bi-polar supply.

Equipment Interfaces

To automate a process of applying desired magnetic fields and capturing images a computer was used to communicate with the external devices. For a power supply we chose to use a Kepco BOP 20-10M as seen in Figure 16. This is a ± 20 volt ± 10 Amp Bi-polar power supply controlled by a BIT-232 serial interface card. Its bi-polar ability helped us easily obtain positive and negative fields. Kepco does provide LabVIEW drivers for all interface cards except the BIT-232. So as we did with the camera, we were forced to create our own LabVIEW drivers. We later found out why BIT-232 interface card was an unpopular item for Kepco. Something happens with the serial buffer when sending commands to devices and certain characters are dropped. For our application we were able to program around this to the best of our ability. When a character is dropped from a text command, the command is not recognized and nothing happens. When a second or third significant digit is dropped from a command it doesn't affect the voltage much. However, when a negative sign or a decimal point is omitted, it causes a temporary extreme change in the current. We minimized the amount of commands that needed to be issued in our control loop by adding a tolerance to the desired field. This problem can be easily corrected in the future by replacing the BIT-232 interface card with a GBIP one and altering some of the block diagram to use part of Kepco's distributed LabVIEW drivers.

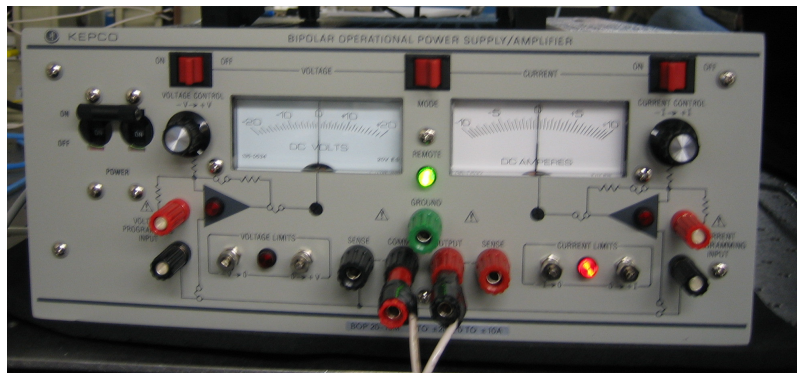


Figure 16: Kepco BOP 20-10M Bi-polar Power Supply

The Gaussmeter used to measure our applied magnetic field is a Lakeshore model 421 (Figure 17). This device is also controlled by RS-232 (serial) communication but it was designed that way. We were able to extract the appropriate parts from the distributed Lakeshore LabVIEW drivers for reading fields and configuring this device.



Figure 17: Lakeshore 421 Gaussmeter

Control Loop

To collect a Kerr image from our microscope, an image must be taken in a saturation field and in a zero field. The first step in automating this process was to create a control loop between the Power Supply and the Gaussmeter. With there being only two user inputs to our front panel GUI we used LabVIEW to create a 2-state case statement within a while loop. One case is entered when the desired field (user input 1) is within the given tolerance (user input 2). In this case, no action is taken and the while loop continues to run while checking the actual field each time. If the user changes the desired field, the loop enters the second case where the difference between the desired field and the actual field is multiplied by a correction factor and added the previous current setting which is held in a shift register. We were able to use this method of adjusting because within the approximate range of 500 to -500 Gauss, the relation of Gauss/Current was relatively linear. This control loop runs quickly and efficiently enough for this stepping method of adjusting to work well. This magnetic field control system was integrated into the automated process that obtains Kerr images.

Camera Interface

The camera chosen for our system is the Scion CFW1312M digital CCD camera. This camera was chosen because of its ability to capture 12-bit monochrome images as opposed to the typical 8-bit capture of most CCD cameras, as well as its optimization toward low light imaging. The additional bit depth allowed us a wider dynamic range in which to apply a scale after the image subtraction. The low light optimization is important because as described in the optics section, after the polarized light is reflected up and passes through the analyzing lens most of the light is extinguished and all that is allowed to pass is the light altered by the Kerr effect which will be very small in comparison. For these reasons this camera worked very well in our application

One disadvantage of this camera we discovered after receiving it is that there are no readily available LabVIEW or MatLAB drivers for it. The manufacturer provides a driver that works with a number of supported software packages, however none of these packages allow for integration with image processing or the other interfaces of our system. After working with the manufacturer and talking to National Instruments, we were able to develop our own drivers in LabVIEW using the camera's software development kit. While this provided a tremendous challenge to our group, we were able work through it and get the camera working with our GUI.

Digital Image Processing

As discussed in the Results section of this report, after acquiring images of our samples, there was nothing to suggest any underlying magnetic structure; however after subtracting images taken at a saturated field from images taken at a zero magnetic field, magnetic domains are clearly visible. This was the underlying reason for digital enhancement of our images; however after short investigation it was concluded that more involved techniques would be necessary. In order to enhance the contrast of this distinction we have taken a number of different approaches through trial and error.

The Center of Microwave Magnetic Materials and Integrated Circuits at the beginning of our project had asked that we make the image processing of this system adaptable. They wanted to have the ability to go in to our system and change the image processing techniques used to better suit their needs for individual experiments. The processing also needed to be fully integrated into our system, for this reason MatLAB was chosen as the means best suited. MatLAB has the ability to integrate with our LabVIEW graphical user interface as well as the power to implement many common practice image processing methods which are currently used by the Center. This solution provided us with the flexibility to adjust our own image processing throughout the project as well as leaving the Center a very adaptable method to run their experiments using our existing software.

In practice our basic image processing consisted of an image subtraction (saturated field image from zero field image) followed by median filtering and grayscale adjustment to enhance the contrast between the oppositely magnetized regions within the sample while ignoring the imperfections of the sample itself. These images showed promising signs of Kerr images; however they were quite noisy with high sensitivity to the amount of time between the capture, camera exposure, and surrounding lighting conditions. To improve upon these images we began capturing multiple images in succession and averaging. We found significant improvement with five averages. As a means to help further reduce noise and any optical speckle effects we introduced a two-dimensional convolution of our subtracted image with an equally balanced square array which had the effect of averaging each pixel with its surrounding pixels. This technique was suggested by Professor Charles DiMarzio. The result produced very clean domain images as shown in the results section of this report.

User Interface

Imaging of magnetic domains using the magneto-optical Kerr effect is not an intuitive task. The end user of our microscope will have some background knowledge of magnetics, optics, and image processing; therefore our user interface must have a great deal of flexibility to allow the user to change parameters based on individual experiments. On the other hand our end user may not have great knowledge about our exact system components (camera, power supply, gauss meter, etc...); therefore we must automate this process within our system. This was the challenge of creating a user interface for our microscope.

LabVIEW was chosen as the software with which to write our interface for several reasons; first it is relatively well known by the Center of Microwave Magnetic Materials and Integrated Circuits for whom the microscope is being built, second it is very easy to follow the logic of this software through the block diagram view of its interface, and third because it is the method our team felt provided us with the most flexibility versus functionality for what we were trying to accomplish. A screen capture of our GUI is shown in Figure 18.

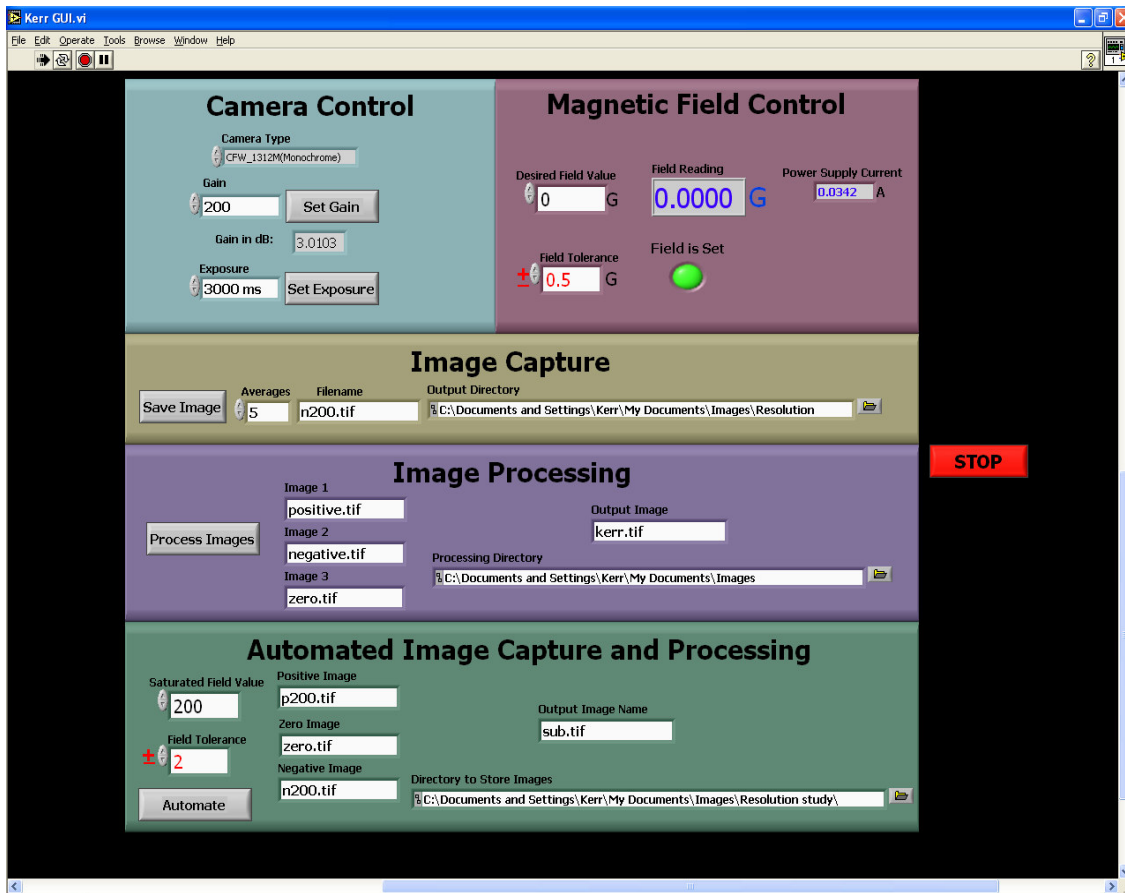


Figure 18: Software User Interface

As seen in Figure 18 above, the interface allows for individual control over the camera functions, the field control, the image capture, and the image processing, as well as a section to perform automated image capture and processing to obtain basic domain images. The upper right section controls the magnetic field; it requires an input of the desired field strength and the tolerable amount of error. It provides an LED to notify the user that the field condition requested is set and displays the current this requires from the power supply. The upper left section of the GUI controls the camera functions (gain and exposure), while there are other functions the camera can be set to control, these are the only two we found useful to this type of imaging. Below these sections is the image capture section which captures as many images as are required by the number of averages, saves these images to temporary files, then averages them together and saves them in the directory selected with the filename requested. The image processing section

allows the user to automatically load up to three images into MatLAB and process them using a pre-written MatLAB Script. This allows for adaptability with as little effort as necessary.

The Automated Image Capture and Processing window (the bottom section of the GUI shown in Figure 18) is a process implemented to allow for easy capture a basic domain image. The need for this level of ease is to allow for alignment of samples, experimentation to find the saturation of a sample, and for confirmation that Kerr images are producible given the current setup. It was used routinely in our experimentations to improve the image processing and alignment of our system as well as to demonstrate the validity of our results. The process works by taking a saturation field level (entered by the user) and capturing images in rapid succession at zero field and both positively and negatively saturated fields. It saves all of these images, performs an image subtraction of the zero field from the positive field as well as the zero field from the negative field, then adds an enhanced color scale and displays both images.

Sample Preparation

To verify the operation of our design experimentally we decided to use Cobalt Zirconium Tantalum alloy ($\text{Co}_{91}\text{Zr}_3\text{Ta}_6$), a soft magnetic material ideally suited for magnetic recording heads, integrated inductors, and other applications. This material was developed by Professor Nian Sun, one of the advisors to our Capstone Design project and a faculty member of CM₃IC. The alloy was deposited in a plasma sputtering process onto glass substrate. Since magnetic domain walls are very likely to occur near magnetic discontinuities, such as edges of the film or surface imperfections, we decided to pattern the film into microscopic structures with well defined edges and corners using a photolithographic process.

Patterning of the sample was carried out at the CM₃IC facilities. To avoid unnecessary expenses and extensive lead times associated with fabricating a custom Chromium on glass photolithographic masks we decided to create our mask using conventional transparency and laser printer. The mask was designed using Deneba Canvas 8.0.1 software and printer on a regular Hewlett Packard 600 dpi laser printer. Figure 19 shows a magnified image of the mask with various patterns we were interested in fabricating. Since the dimensions of magnetic domains are directly proportional to dimensions of the magnetic sample we decided to fabricate several square features with 200-600 μm sides.

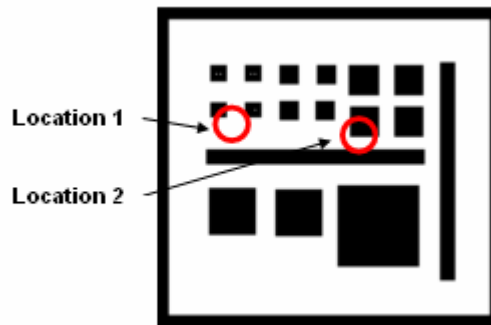


Figure 19: Photolithographic mask

In the first step of the photolithographic process 7 μm positive photoresist was deposited onto the magnetic sample by using Chemat Spin-Coater. The substrate was then pre-baked for 2 minutes at 115 $^{\circ}\text{C}$. A Kasper Wafer Alignment System was then utilized to expose the substrate covered with the photolithographic mask from Figure 19 to intense UV radiation. The sample was then post-baked for 2 minutes at 115 $^{\circ}\text{C}$ and developed using MF-319 positive developer. Patterning was performed using a wet etch process with a 1:1:1 combination of HCl (Hydrochloric), HNO₃ (Nitric), and C₂H₄O₂ (Acetic) acids. Finally, the remaining photoresist was removed by applying Acetone to the surface of the sample. As a result $\text{Co}_{91}\text{Zr}_3\text{Ta}_6$ film was removed from the entire glass substrate with the exception of areas protected from UV exposure by the opaque areas of the photolithographic mask. The patterned sample was then used to verify the operation of the MOKE Microscope.

Results and Discussion

Patterned $\text{Co}_{91}\text{Zr}_3\text{Ta}_6$ film was used to conduct proof of concept study of the MOKE Microscope. The sample was placed on a Si (Silicon) wafer and positioned on top of the electromagnet such that the fringing magnetic field could be used for biasing during MOKE imaging. The alignment and calibration of the optical system has proven to be a complicated and tedious task since MOKE contrast can only be achieved with the optical system aligned for optimal polarization extinction. Such condition was achieved by varying the position of the output face of the optical fiber relative to the collimating and focusing lenses. Since the output face of the fiber was mounted via a FC to SM1 adapter within a lens mount positioned on a three dimensional micrometer stage fine translational adjustments on the order of microns were possible.

Kerr images are not immediately seen in the images captured by the camera. Consequently, image processing software was required to capture, accumulate, and subtract images under different magnetic biasing conditions. First MOKE images were captured from Location 1 in Figure 19 as shown in Figure 20.

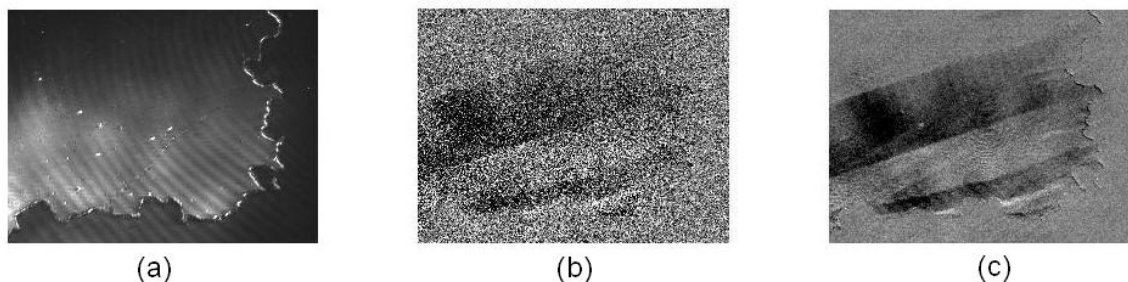


Figure 20: (a) Raw image, (b) Background subtracted image, (c) Digitally processed image

Image (a) in Figure 20 is the raw image captured by the camera with applied field of 40 Gauss. 40X objective was used and the field of view (the physical dimensions in image plane) in this case is $190 \times 155 \mu\text{m}^2$. There is no information in this image to suggest any underlying magnetic structure. The non-uniformity of the illumination in the image is due to imperfect alignment of the input laser light coupling optics and the circular diffraction pattern is likely to be a result of a standing mode in the polarizing beam splitter or the protective coating on the CCD chip of the camera. However, when another image is captured with 0 Gauss applied field and subtracted from image (a) to produce image (b) in Figure 20 strips of varying light intensity become visible. These strips are in fact magnetic domains in the $\text{Co}_{91}\text{Zr}_3\text{Ta}_6$ film and the boundaries of these strips are magnetic domain walls.

While this result is very exciting because it confirms the ability of our design to visualize the magnetic properties of the sample under investigation the resulting image is very noisy and low in contrast. Significant improvement was achieved with digital signal processing techniques as shown in Figure 20 (c). This image was achieved from image (b) by applying median filtering, 2D convolution, and grayscale adjustment functions in the Image Processing Toolbox of MatLAB 7.1 software. In image (c) magnetic domain

structures are clearly seen. Alternating dark and bright stripes correspond to regions of unidirectional magnetization in the opposite direction.

As discussed in the Magnetic Domains section of this report, these structures are governed by minimization of energy in the system eliminating high concentration of magnetic poles on the edges of the sample. From image (c) we can determine the easy axis of the material defined as the preferred direction of the magnetization in the absence of applied field. The direction of magnetic domains in the image indicates that the easy magnetization axis is at a small angle to the bottom edge of the rectangular film structure. Image (c) proves the ability of our microscope to detect magnetic domain structures in magnetic materials by utilizing Kerr rotations as discussed in the Magneto-Optical Kerr Effect section of this report.

Additional images of magnetic domains were captured at Location 2 in Figure 19. These images are shown in RGB colormap in Figure 21 alongside images captured from Location 1.

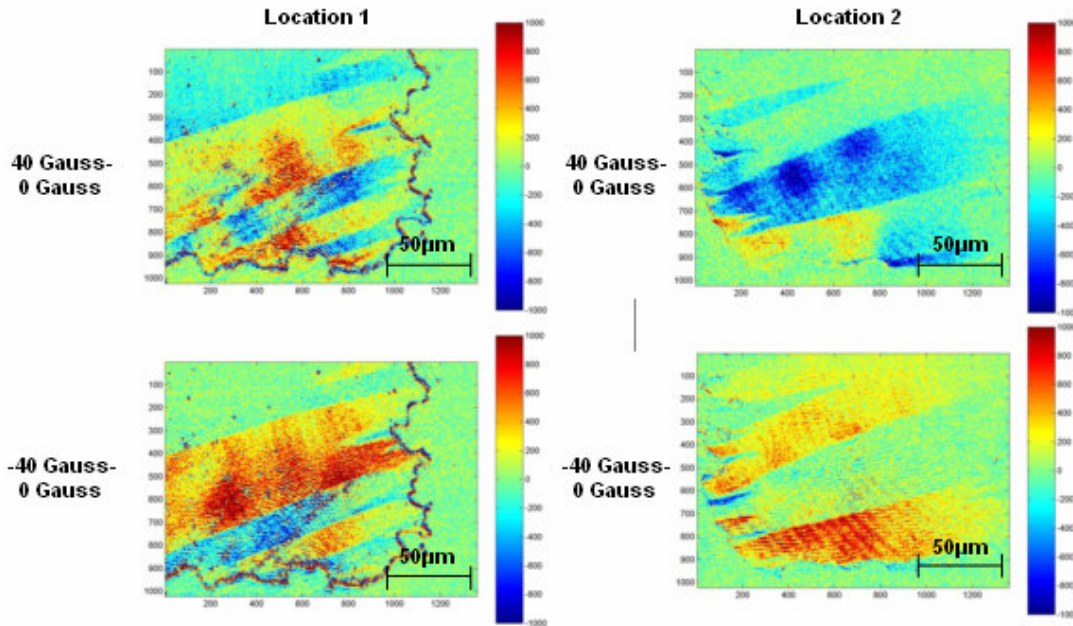


Figure 21: Magnetic domain images shown in RGB colormap

Once again, magnetic domains appear as strips of varying intensity at a small slope with respect to the bottom edge of the square magnetic structure indicating the direction of the easy magnetization axis. Top two images were obtained by first capturing a picture of the magnetic structure under a positive biasing field of 40 gauss, and then subtracting the background signal with 0 Gauss applied field. As shown in Figure 21 the average intensity in these images is lower as indicated by prevalently blue colors. In the two bottom images a picture of the magnetic structure with a negative biasing field of -40 Gauss was captured first, followed by subtraction of 0 Gauss background. The intensity in these images is higher as indicated by the prevalence of red colors. Based on this

observation we can conclude that our design has the ability of optically characterizing the behavior of a magnetic material in response to change in biasing conditions.

Summary

In this report we've shown that our design is capable of optically visualizing domain structures of magnetic materials. We have also shown that our design acts as an optical magnetometer mapping magnetization variations in the surface of the sample into light intensity variations in the resulting images. This design allows localized probing of magnetic properties of the sample on a micro scale with ultimate resolution of $<0.8\mu\text{m}$. This capability is very important in the development of magnetic materials and devices since most thin film fabrication techniques, such as plasma sputtering, pulsed laser deposition, liquid phase epitaxy, etc. often result in non-uniform magnetic properties in the entire area of the deposited film. Hence it is important to probe the magnetic structure of deposited films locally to characterize the spatial variation of magnetic properties. This information can then be used to optimize the deposition process and improve the uniformity of deposited samples. Furthermore, the magnetic domain state of the sample is often a critical parameter in the design of high performance magnetic devices such as magnetic recording heads, integrated inductors, magnetic sensors, and spintronic devices.

In the Results and Discussion section of this report we've shown how all subsystems of our design are necessary to produce MOKE images. A well adjusted polarizing optical system, custom machined microscope components, computer controlled electromagnet, computer interface, and finally image processing software all play an important role in the process of Magneto-Optical characterization of magnetic materials. The microscope is currently ready to be used by the researchers at CM₃IC and we hope that it will promote further development of science and technology there.

Acknowledgements

The design team would like to thank Professor Charles DiMarzio for making this project possible by sharing his extensive experience in electromagnetics and contributing to each aspect of our design. We'd like to thank the students and staff of the Optical Science Lab for their interest in our project and willingness to share their knowledge and equipment with our group.

The design team would also like to thank Professor Nian Sun for sharing his experience in magnetism, magnetic materials, and MOKE microscopy with the group and contributing ideas to each stage of the project. We'd like to thank the students and staff of the Center of Microwave Magnetic Materials and Integrated Circuits for their interest in our project, for their valuable advice in designing different subsystems of our microscope, and willingness to share equipment with the group.